12^{th} International Conference on Fracture Mechanics of Concrete and Concrete Structures
FraMCoS-12
B.L.A. Pichler, Ch. Hellmich, P. Preinstorfer (Eds)

https://doi.org/10.21012/FC12.1370
PL1

SPRAIN ENERGY AND GAP TEST CONSEQUENCES FOR DAMAGE LOCALIZATION AND FRACTURE MECHANICS

ZDENĚK P. BAŽANT[1,*], HOULIN XU[2], ANH TAY NGUYEN[3] AND YANG ZHAO[2]

[1] Presenter (plenary); McCormick Institute Professor and W.P. Murphy Professor of Civil and Mechanical Engineering and Materials Science, Northwestern University, 2145 Sheridan Road, CEE/A135, Evanston, IL 60208
[2] Department of Civil and Environmental Engineering, Northwestern University, Evanston, IL 60208
[3] Department of Mechanical Engineering, Northwestern University, Evanston, IL 60208

[*] e-mail: z-bazant@northwestern.edu

Key words: fracture energy, fracture and damage mechanics, second displacement gradient, material rotation gradient, spress–sprain relation

Abstract. The smooth Crack Band Model (sCBM), conceived in 2021, incorporated a novel localization limiter that is imposed on the 'sprain' field, representing the second-gradient of displacement, to prevent spurious damage localization during fracture growth. A following study in 2023 presented an improved model, called the smooth Lagrangian Crack Band model (slCBM), in which the term "spress" was introduced as the force variable work-conjugate to the "sprain" tensor. More importantly, the numerical difficulty of the sCBM due to using the nodes of adjacent finite elements was overcome by treating displacement vectors and their gradients as independent fields with C_0 continuity in finite element implementation, constrained by second-order tensorial Lagrange multipliers. Combined with the microplane model M7 for triaxial softening damage, our numerical validation of the gap test results using the slCBM demonstrates accurate reproduction of size effects under varying crack-parallel stresses. The same, though with path-dependence limitations, is achieved by a simple formula for predicting the crack-parallel stress effects on the fracture energy. Traditional line crack models, including their phase-field reincarnation, give errors of up to 100%. Further it is demonstrated that the existing strain-gradient theories, lacking the resistance to material rotation gradients, predict incorrect fracture patterns with load errors up to 55% error in the case of Mode II and III fractures and for Mode I fractures mixed with shear loading. The crack-parallel stress effect appear to be universal for all materials, including atomistically sharp crystal cracks. There are fundamental implications for the theory of fracture mechanics.

1 INTRODUCTION

Traditionally, the fracture energy was believed to remain constant as a material property. However, a simple groundbreaking experiment known as the gap test, conceived in 2020 [1], demonstrated that the fracture energy of concrete is not a constant but varies by as much a 100% or more as a function of crack-parallel normal stresses. This phenomenon has subsequently been confirmed in other quasibrittle material such as fiber-polymer composites [2] and fiber-reinforced concrete (FRC), and probably exists for all materials. Ongoing MD simulations indicate that it also occurs atomistically sharp cracks in crystals.

In 2023, the new concept of sprain energy and sprain forces derived from it [3] was pro-

posed to avoid the mesh sensitivity issues of a softening damage constitutive law and to reproduce the correct sensitivity to crack parallel stresses (the term "sprain" was borrowed from medicine where it means the damage to a ligament over a finite length without any break). Curvature resisting sprain forces were derived from the sprain energy and applied on the nodes of a FE mesh. But some of the sprain forces had to be applied on the nodes of adjacent finite elements, which increased the running time of the FE program by an order of magnitude and complicated programming.

To overcome this problem, a groundbreaking method called the smooth Lagrangian crack band model (slCBM) was formulated. It was based on curvature-resisting spress-sprain relations. The purpose of the spress was to resist the curvature (or the hessian) of the vectorial displacement field in the softening damage zone (the term "spress" tensor denoted the derivative of the total energy density with respect to the sprain tensor). This approach allowed both the displacements and their gradients to be represented by linear shape functions of C_0 continuity, constrained by a second-order Lagrange multiplier tensor. In this way, the need for using the nodes of the adjacent elements was eliminated. This achieved high computational efficiency.

2 SPRAIN ENREGY DENSITY

The basic hypothesis of this new theory is that the Helmholtz energy density in the continuum is a sum of two terms, the second term augmenting the standard expression:

$$\bar{\boldsymbol{\Psi}}(\boldsymbol{\epsilon}, \boldsymbol{\xi}) = \boldsymbol{\Psi}(\boldsymbol{\epsilon}) + \boldsymbol{\Phi}(\boldsymbol{\xi}) \tag{1}$$

where $\boldsymbol{\Psi}(\boldsymbol{\epsilon})$ represents the standard strain energy density and $\boldsymbol{\Phi}(\boldsymbol{\xi})$ denotes the sprain energy density. Here $\boldsymbol{\epsilon}$ is the strain tensor and $\boldsymbol{\xi}$ is the sprain tensor, both dimensionless; $\boldsymbol{\eta}$ is used to represent the strain gradient tensor (with dimension m^{-1}). In Cartesian coordinates x_i (where $i = 1, 2, 3$ for 3D, or $i = 1, 2$ for 2D), its components are defined as:

$$\begin{aligned} \xi_{ijk} &= l_0 u_{i,jk}, \quad \eta_{ijk} = \epsilon_{ij,k} \\ u_{i,jk} &= \eta_{ijk} + \omega_{ij,k} \end{aligned} \tag{2}$$

(the subscripts following a comma indicate partial derivatives). The displacement vector components are denoted by u_i, while $\epsilon_{ij} = (u_{i,j} + u_{j,i})/2$ represents the linearized small strain tensor, and $\omega_{ij} = (u_{i,j} - u_{j,i})/2$ describes the material rotation tensor (corresponding to small strain tensor). l_0 is the material length characterizing the size of the fracture process zone (FPZ).

The energy framework of the model is complemented by three essential relationships:

$$\boldsymbol{\Phi}(\boldsymbol{\xi}) = \int s_{ijk} \mathrm{d}\xi_{ijk}, \tag{3}$$

$$s_{ijk} = \frac{\partial \boldsymbol{\Phi}(\boldsymbol{\xi})}{\partial \xi_{ijk}} \tag{4}$$

$$s_{ijk} = \kappa \big\langle\, |\boldsymbol{\xi}| - C \,\big\rangle\, \xi_{ijk}/|\boldsymbol{\xi}| \tag{5}$$

where $\boldsymbol{\Phi}(\boldsymbol{\xi})$ is a function of the dimensionless third-order tensor $\boldsymbol{\xi}$. Parameter κ represents the sprain stiffness, while $|\boldsymbol{\xi}|$ denotes an appropriate norm of $\boldsymbol{\xi}$ (typically $\|\boldsymbol{\xi}\|_2$). The threshold C determines the value below which the effects of displacement field curvature on damage become negligible, which is a condition that prevails in most of the structure volume. In that volume the classical continuum mechanics, with no sprain energy, applies.

spress-sprain relation in Eq. (5) has a different purpose than the stress-strain constitutive relation. Its purpose is essentially geometric in nature—to limit the displacement curvature as required by material heterogeneity.

3 TENSORIAL LAGRANGE MULTIPLIER CONSTRAINING APROXIMATE DISPLACEMENT GRADIENT

The generalized potential of the structural system can be expressed as:

$$\Pi(\boldsymbol{u}, \boldsymbol{\zeta}, \boldsymbol{\lambda}) = W_{in} - W_{ex} \tag{6}$$

where the internal energy W_{in} and the external energy W_{ex} are defined as [4]:

$$W_{in} = \int_V \mathbf{\Psi}[\boldsymbol{\epsilon}(\mathbf{u})]\,\mathrm{d}V + \int_V \mathbf{\Phi}[\boldsymbol{\xi}(\boldsymbol{\zeta})]\,\mathrm{d}V - \int_V \boldsymbol{\lambda}(\nabla\mathbf{u} - \boldsymbol{\zeta})\,\mathrm{d}V \tag{7}$$

$$W_{ex} = \int_V \mathbf{f}(\mathbf{x}) \cdot \mathbf{u}\,\mathrm{d}V \tag{8}$$

In the last equation, we introduced a separate dimensionless second-order tensor field, $\boldsymbol{\zeta}$, which approximates the actual displacement gradient $\nabla\mathbf{u}$. It is constrained to it in a weak sense by means of the tensorial Lagrange multiplier $\boldsymbol{\lambda}$, which is a variable throughout the structure. The sprain tensor $\boldsymbol{\xi}$ is then represented through the first gradient of $\boldsymbol{\zeta}$ multiplied by the characteristic length l_0

$$\boldsymbol{\xi} = l_0 \nabla \zeta \tag{9}$$

This formulation provides a comprehensive framework for analyzing material behavior during fracture. It incorporates both traditional strain energy and the novel sprain energy components, and requires only a modest generalization of a program for the crack band model (CBM).

4 COMPUTATIONAL IMPLEMENTATION AND OPTIMIZATION

The three-dimensional implementation of our model presents another computational challenge. The full formulation requires 21 degrees of freedom (DoFs) per node: 3 DoFs for displacement $\boldsymbol{u}$, 9 for displacement gradient $\nabla\boldsymbol{u}$, and 9 for the independent gradient field $\boldsymbol{\zeta}$. For an 8-node 3D brick element, this amounts to 168 DoFs, demanding substantial computational resources.

To make the computations more tractable, we developed two optimization strategies. First, we can implement a staggered solution scheme in which we postpone the updating of the Lagrange multiplier tensor to the subsequent load step or iteration. Thus the number of DoFs per element gets reduced to 96, which is manageable.

Second, and more effectively, we can exploit the physics of crack propagation by knowing that the curvature (sprain) threshold C is typically exceeded only in the (x, y) plane, where x represents the crack propagation direction and y the crack in-plane normal direction. This allows us to simplify the formulation to:

$$\boldsymbol{u} = [u, v, w]_{1\times 3} \quad \boldsymbol{\zeta} = [\zeta_{ij}]_{2\times 2} \quad \boldsymbol{\lambda} = [\lambda_{ij}]_{2\times 2} \tag{10}$$

where $i, j \in 1, 2$. This computational optimization reduces the number of DoFs per node to 11 (i.e., to 88 per 8-node brick element). This provides an efficient computation for common test configurations such as the three-point-bend (3PB) specimen (shown in Fig 2A), the gap test, and the four-point-bend (4PB) shear tests, while the computations remain exact when the threshold C is not exceeded in the (x, z) and (y, z) planes.

Our numerical implementation, validated across multiple platforms (COMSOL, Matlab, and Abaqus), employs weak variational equations derived from the energy functional. COMSOL proves particularly effective for postpeak softening simulations under crack mouth opening displacement (CMOD) control, while the applied load is treated as a global unknown.

The model leads to consistent displacement fields in both static and explicit dynamic analyses, despite the absence of time-dependent evolution equations for $\boldsymbol{\zeta}$ and $\boldsymbol{\lambda}$. For optimal mesh design, our smooth spress-sprain relation indicates that the element size, h, should be $h \approx l_0/6$, where l_0 is the material characteristic length determined through scaled size effect tests [5]. The sensitivity analysis in Fig. 2D illustrates how varying the threshold parameter C affects the results.

5 INABILITY OF CLASSIC STRAIN-GRADIENT DAMAGE MODELS TO PREDICT FRACTURE WITH SHEAR

The diversity and multitude of the fracture tests of concrete offers an ideal testing ground

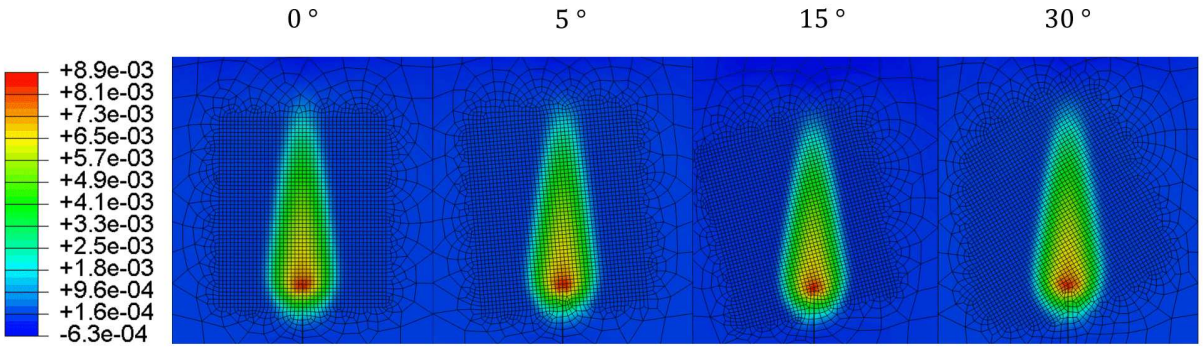

Figure 1: Rotating the square FE mesh in slCBM by 5° to 30° produces identical results.

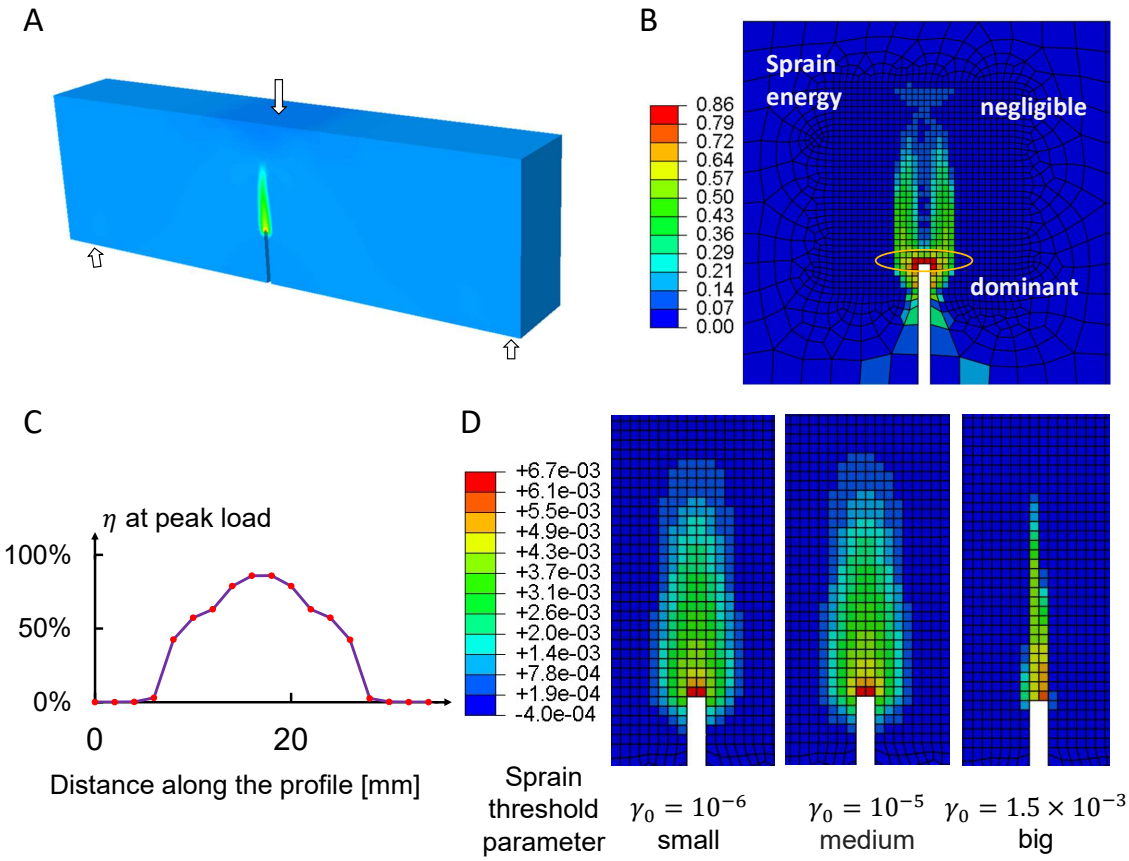

Figure 2: (A) Near-notch damage zone in a symmetric 3PB test specimen using 3D slCBM with the (x, y) plane curvature control: 3-Point Bend test specimen (3PB). (B) Map of sprain energy intensity in the near-notch region. (C) Profile of sprain energy density ratio η across the damage band front (η = sprain energy density / total energy density); the curvatures at both ends are not restricted because $\eta <$ threshold. (D) Near-notch strain profiles for three cases of threshold parameter: 10^{-6},10^{-5} and 1.5×10^{-3} (on the right, the threshold is too large to limit curvature, which makes the situation equivalent to the original crack band model, CBM).

for fracture models of different types. Comparisons with eleven different loading configurations demonstrated that peridynamics is merely a fiction, unable to reproduce most experimental data from the literture [6] (except for a few "nondistinctive" test [7] which can be fitted by most models and thus prove nothing). Likewise, while the recent fad of phase-field fracture can reproduce well the linear elastic fracture mechanics (LEFM) it can do so only in absence

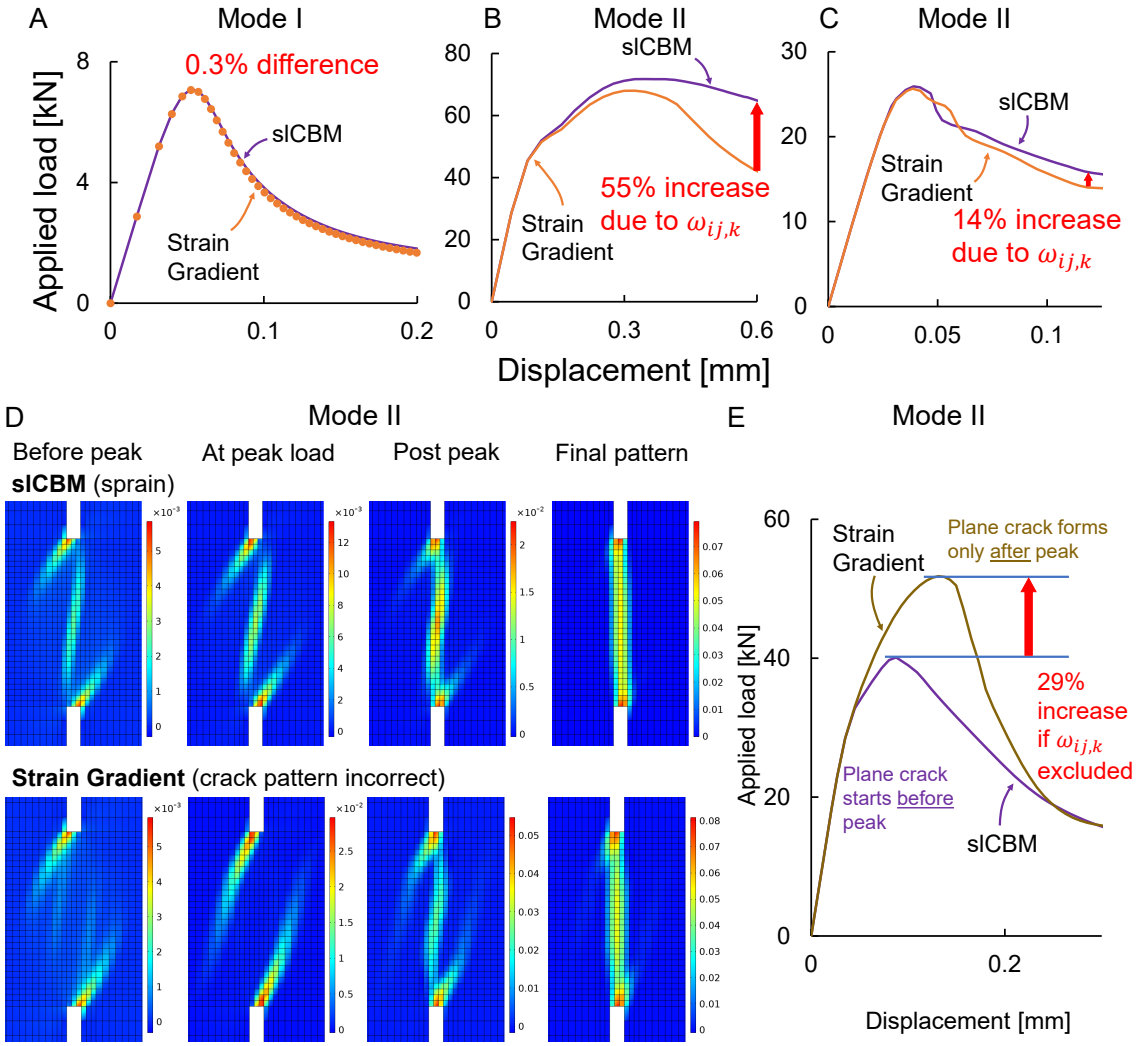

Figure 3: Comparisons of the slCBM with the Strain Gradient theory: (A) In symmetric fracture tests such as 3PB, the responses obtained from both models differ negligibly because the rotation gradients in the notch line vanish and on its sides are usually not big enough to exceed the threshold. (B,C) These are Mode II four-point-bend (Iosipescu) shear tests with two different constitutive laws – scalar damage law and Grassl's constitutive for concrete (which is CDPM law featured in software COMSOL). The material rotation gradients on the notch line are significant and increase in postpeak. (D,E) The absence of $\omega_{xy,x}$ in strain-gradient model leads to different fracture pattern evolution. After exceeding threshold C= $5 \cdot 10^{-5}$, κ was kept constant; κ = 1 MPa in (A); κ = 0.11 MPa in (B); κ = 0.105 MPa in (C); κ = 0.01 MPa in (D,E).

of crack-parallel stresses, which is a rare case practical situations. This renders the phase-field model almost useless. The same can be said of all cohesive crack models.

Recently, though, the strain gradient damage models were shown to be effective for Mode I opening fractures. Nevertheless, these models have an Achilles heel—fracture caused by shear or accompanied with shear loading.

The incorporation of strain gradients into material constitutive equations originally served a specific purpose: to create a homogenized model of elastic microstructures that included additional localized degrees of freedom [8–10]. To check the difference between the strain-gradient damage model [11–13] and the present sprain model, we exploit the fact that the former is obtained as a special case of the latter when the displacement gradient is symmetrized in the coding [14]. That way we can use the same material constitutive model for both cases, which is essential for a mean-

ingful comparison. The symmetrization means that the gradient of material rotation is not resisted, which intuitively explains why in (Fig. 3A-C) the train gradient model markedly underestimates the stiffness.

Our comparative simulations of 3PB Mode I and 4PB Mode II fracture tests (Fig. 3A-E) reveal three findings: 1) Under symmetric loading conditions (Mode I fracture), where the crack line serves as the deformation symmetry axis, both models produce nearly identical results. 2) The slCBM captures distinct crack evolution patterns, detecting plane crack formation before peak load due to its enhanced sensitivity to rotation gradients. 3) In shear or mixed-mode scenarios, the slCBM predicts significantly higher loads - up to 55% greater than the strain-gradient model.

Similar or even stronger differences may be expected for Mode III fracture under torsional loading.

6 CONCLUSIONS

1. The slCBM demonstrates superior accuracy in reproducing experimental results from gap tests, size effect tests, and Mode II shear tests on quasibrittle materials. This is a significant improvement over traditional line crack models, the phase field included [6].

2. The damage zone width at crack band front varies with the crack-parallel stress while remaining governed by a material characteristic length, which is a material constant.

3. The strain-gradient damage theories omit resistance to the material rotation gradients. This is not important for Mode I fracture but causes major errors for Mode II and III fracture as well as for combinations of Model I with shear loading as in shear failure of reinforced concrete beams. An error f 55% in load and wrong predictions of the failure patterns have been documented.

4. The strong influence of crack-parallel stress on fracture energy has been experimentally demonstrated for concrete, fiber-reinforced concrete and fiber-polymer composites, and is also indicated by MD simulations for atomistically sharp cracks in silicon. Probably it exists in all materials.

REFERENCES

[1] H.T. Nguyen, M. Pathirage, G. Cusatis, and Z.P. Bažant. Gap test of crack-parallel stress effect on quasibrittle fracture and its consequences. *Journal of Applied Mechanics*, 87(7):071012, 2020.

[2] J. Brockmann and M. Salviato. The gap test–effects of crack parallel compression on fracture in carbon fiber composites. *Composites Part A: Applied Science and Manufacturing*, 164:107252, 2023.

[3] Y. Zhang and Z.P. Bažant. Smooth crack band model—a computational paragon based on unorthodox continuum homogenization. *Journal of Applied Mechanics*, 90(4):041007, 2023.

[4] A.T. Nguyen, H. Xu, K. Matouš, and Z.P. Bažant. Smooth lagrangian crack band model (slcbm) based on spress-sprain relation and lagrange multiplier constraint of displacement gradient. *Journal of Applied Mechanics*, pages 1–19, 2023.

[5] Z.P. Bažant, J.L. Le, and M. Salviato. *Quasibrittle Fracture Mechanics and Size Effect: A First Course*. Oxford University Press, 2021.

[6] Z.P. Bažant, H.T. Nguyen, and A.A. Dönmez. Critical comparison of phase-field, peridynamics, and crack band model m7 in light of gap test and classical fracture tests. *Journal of Applied Mechanics*, 89(6):061008, 2022.

[7] Z.P. Bažant and H.T. Nguyen. Proposal of m-index for rating fracture and damage models by their ability to represent a set

of distinctive experiments. *Journal of Engineering Mechanics*, 149(8):04023047, 2023.

[8] E. Cosserat and F. Cosserat. *Théorie des corps déformables (Theory of deformable bodies)*. A. Hermann & Fils, 1909.

[9] R. Toupin. Elastic materials with couple-stresses. *Archive for rational mechanics and analysis*, 11(1):385–414, 1962.

[10] R.D. Mindlin. Micro-structure in linear elasticity. *Archive for rational mechanics and analysis*, 16:51–78, 1964.

[11] R. de Borst and C.V. Verhoosel. Gradient damage vs phase-field approaches for fracture: Similarities and differences. *Computer Methods in Applied Mechanics and Engineering*, 312:78–94, 2016.

[12] M.G.D. Geers, R. de Borst, W.A.M. Brekelmans, and R.H.J. Peerlings. Strain-based transient-gradient damage model for failure analyses. *Computer Methods in Applied Mechanics and Engineering*, 160(1):133–153, 1998.

[13] R.H.J. Peerlings, R. de Borst, W.A.M. Brekelmans, and J. de Vree. Gradient enhanced damage for quasi-brittle materials. *International Journal for numerical methods in engineering*, 39(19):3391–3403, 1996.

[14] H. Xu, A.T. Nguyen, and Z.P. Bažant. Sprain energy consequences for damage localization and fracture mechanics. *Proceedings of the National Academy of Sciences*, 121(40):e2410668121, 2024.